Supporting Information

Metal-Organic Framework-Derived 2D Layered Double Hydroxide Ultrathin Nanosheets for Efficient Electrocatalytic Hydrogen Evolution Reaction

Jie Song,[‡a] *Jeng-Lung Chen,*[‡b] *Zichen Xu*[a] *and Ryan Yeh-Yung Lin**[a]

[a] State Key Laboratory of Fine Chemicals, Zhang Dayu School of Chemistry, Dalian University of Technology, Dalian, Liaoning 116024, China

Email: yylin@dlut.edu.cn

[b] National Synchrotron Radiation Research Center, Hsinchu 300092, Taiwan

‡ Jie Song and Jeng-Lung Chen contributed equally to this work.

1. Experimental section

1.1 Materials

Copper chloride dihydrate ($CuCl_2 \cdot 2H_2O$, ≥99.0%) was purchased from Titan Scientific Co., Ltd. (Shanghai, China). Cupric nitrate trihydrate ($Cu(NO_3)_2 \cdot 3H_2O$, 99%), iron nitrate nonahydrate ($Fe(NO_3)_3 \cdot 9H_2O$, 98%), urea (99%), ammonium fluoride (NH_4F, 97%), *N*,*N*-dimethylformamide (DMF, ≥99.9%), methanol (MeOH, 99.9%), ethanol (EtOH, 99.5%), xylene (99%) and H_2PtCl_6 (≥99.9%) were purchased from Energy Chemical Technology Co., Ltd. (Shanghai, China). Iron chloride tetrahydrate ($FeCl_2 \cdot 4H_2O$, ≥99.0%) was obtained from Acros Organics (New Jersey, USA). $NaBH_4$ (AR) was purchased from Damao Chemical Reagent Factory (Tianjin, China). KOH was provided by Aladdin Chemistry Co., Ltd. (Shanghai, China).

1.2 Synthesis of CuFe(dobpdc)

CuFe(dobpdc) was prepared according to the reported literature procedures with slight modifications.[17] Typically, $CuCl_2 \cdot 2H_2O$ (0.17 mmol), $FeCl_2 \cdot 4H_2O$ (0.087 mmol) and H_4dobpdc (0.10 mmol) were added to a 50 mL dried Schlenk flask under N_2. Subsequently, the dry solvent mixture of DMF (10 mL), ethanol (2 mL) and deionized water (1 mL) was injected into the flask and heated at 120 °C for 24 h under N_2. After the reaction, the as-synthesized CuFe(dobpdc) was washed three times with DMF and twice with methanol. Finally, CuFe(dobpdc) was dried at 100 °C under vacuum overnight.

1.3 Synthesis of CuFe-LDHm

CuFe(dobpdc) (60 mg) was immersed in 4.0 M KOH solution (10 mL) for 7 h at 50 °C. The resulting product (CuFe-LDHm) was then washed with deionized water for three times, and dried at 80 °C overnight in a vacuum oven.

1.4 Synthesis of Pt@CuFe-LDHm

CuFe-LDHm (30 mg) was dispersed in 0.5 g L^{-1} H_2PtCl_6 solution (3 mL) for 2 h at room temperature. Then, the mixture solution was centrifuged and washed several times with deionized water and dried at 80 ℃ overnight in a vacuum oven. The vacuum-dried product was immersed in 0.2 M $NaBH_4$ solution (3.0 mL) for 2 h at room temperature. Finally, the obtained product (Pt@CuFe-LDHm) was collected and washed by deionized water and dried at 80 °C overnight in a vacuum oven.

1.5 Synthesis of CuFe-LDHs

$Cu(NO_3)_2 \cdot 3H_2O$ (2.0 mmol), $Fe(NO_3)_3 \cdot 9H_2O$ (1.0 mmol), urea (10 mmol) and NH_4F (4.0 mmol) were dissolved in deionized water (8.0 mL) and then transferred to a 20 mL Teflon® vessel under ultrasonication for 15 min. Then the reaction vessel was put into an oven reacting at 120 ℃ for 6 h. Finally, the product was washed by deionized water for three times and dried at 80 ℃ overnight in a vacuum oven.

1.6 Synthesis of CuFe-LDHs-sheet

CuFe-LDHs (50 mg) was dispersed in xylene and sonicated for 3 days. Then, the product was washed by ethanol for three times and dried at 80 ℃ overnight in a vacuum oven.

1.7 Synthesis of Pt@CuFe-LDHs-sheet

CuFe-LDHs-sheet (30 mg) was dispersed in 0.5 g L^{-1} H_2PtCl_6 solution (3 mL) for 2 h at room temperature. Then, the mixture solution was centrifuged and washed several times with deionized water and dried at 80 ℃ overnight in a vacuum oven. The vacuum-dried product was immersed in 0.2 M $NaBH_4$ solution (3.0 mL) for 2 h at room temperature. Finally, the obtained product (Pt@CuFe-LDHs-sheet) was collected and washed by deionized water and dried at 80 ℃ overnight in a vacuum oven.

1.8 Material Characterizations

PXRD patterns of the prepared electrocatalysts was characterized with a Rigaku SmartLab 9kW powder X-ray diffractometer equipped with a Cu Kα radiation source. FTIR spectra

were obtained using a Shimadzu IRTracer-100 in the range of 400-4000 cm^{-1}. The elemental contents were analyzed by Perkin Elmer Avio 500 ICP-OES. FESEM images were recorded on a NOVA NanoSEM 450 instrument. TEM images and corresponding EDS mappings were recorded on a FEI Tecnai G2F30 S-TWIN field emission transmission electron microscope equipped with energy-dispersive X-ray spectroscope. AFM was conducted on a Bruker Nanowizard 4XP instrument to determine the thinkness of the nanosheets. XPS was performed on a Thermos Scientific K-Alpha+ instrument with an Al Kα excitation source, and the binding energies were referenced to C 1s peak at 284.8 eV. The BET surface areas were calculated from N_2 adsorption/desorption isotherms with a Micromeritics 3Flex instrument at 77 K in liquid N_2 baths and the purity of N_2 gas was 99.999%. Prior to the measurement, the prepared electrocatalysts were activated at 413 K for 18 h under high vacuum.

1.9 X-ray Absorption Spectroscopy Analysis

XANES and EXAFS spectra of Cu and Fe K-edges were recorded with quick-scan method[1] in the transmission mode under ambient conditions at TPS 44A beamline in National Synchrotron Radiation Research Center (NSRRC) in Taiwan. The EXAFS analysis was carried out by performing Fourier transform on k^3-weighted EXAFS oscillations to evaluate the contribution of each bond pair to the Fourier transform peak.

1.10 Electrochemical Measurements

All electrochemical measurements were executed in a three-electrode system using a CHI760E electrochemical workstation (Shanghai Chenhua, China). Platinum plate (1 cm × 1 cm) and Hg/HgO electrode were used as the counter electrode and reference electrode, respectively, and the prepared electrocatalysts served as the working electrode. The working electrode was prepared by the following procedure: 10 mg of prepared electrocatalyst (CuFe(dobpdc), CuFe-LDHm, CuFe-LDHs, CuFe-LDHs-sheet, Pt@CuFe-LDHs-sheet,

Pt@CuFe-LDHm and Pt/C) and 3 μL of 5wt% Nafion solution were added into 2 mL of THF, followed by ultrasonication for 1 h to form a homogeneous catalyst ink. Then 20 μL of the prepared ink was dropped on the surface of the NF (1 cm × 1 cm) and dried at 80 ℃ in a vacuum oven for 1 h. 1.0 M KOH, 0.1 M KOH and 1.0 M PBS were used as the electrolytes which were purged with N_2 for 30 min. Before the electrochemical tests, the working electrode undertook 30 cycles of CV at a scan rate of 50 mV s^{-1} to reach a stable state. LSV curves were carried out with a scan rate of 5 mV s^{-1}. The potentials referred to the reversible hydrogen electrode (RHE) were calculated according to the equation: $E_{RHE} = E_{Hg/HgO} + 0.059 \times pH + 0.098$ V. The Tafel slopes were calculated with the following equation: $\eta = b \times \log j + a$, where η is the overpotential, j is the current density, and b is the Tafel slope. EIS measurements were recorded in the frequency range of 10^5 Hz to 0.1 Hz with an amplitude of 5 mV. ECSA of the electrocatalysts were evaluated using C_{dl} measured by CV in the non-faradaic region.

2. Supplementary Figures

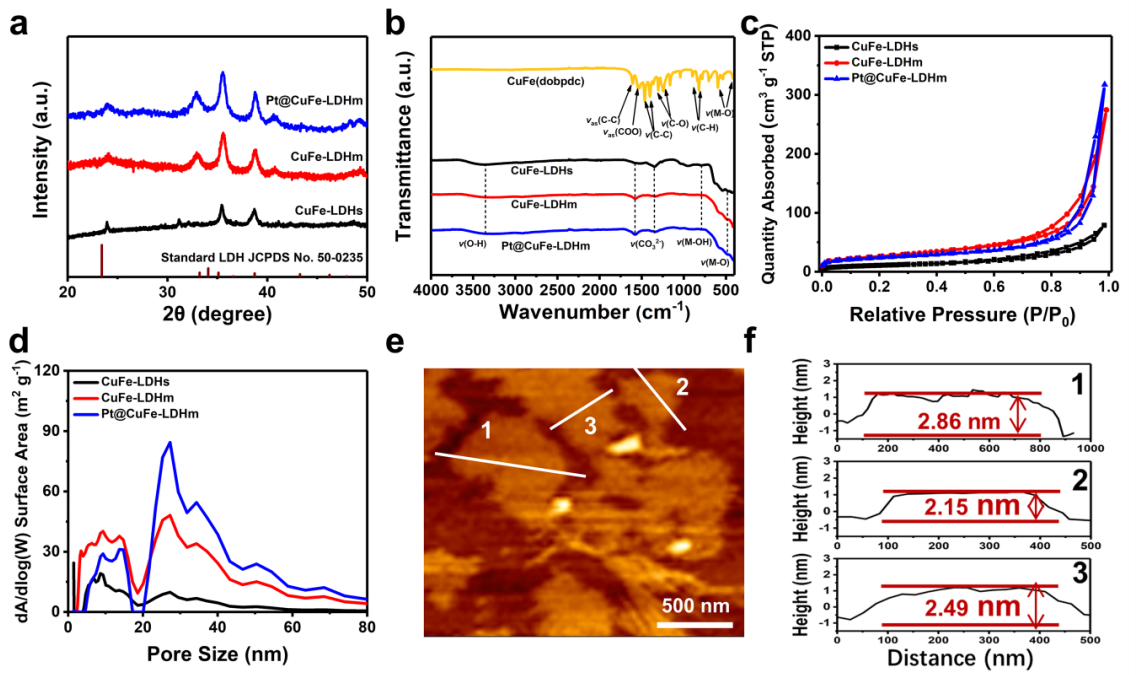

Fig. S1. (a) PXRD patterns of CuFe-LDHs, CuFe-LDHm and Pt@CuFe-LDHm. (b) FTIR spectra of CuFe(dobpdc), CuFe-LDHs, CuFe-LDHm and Pt@CuFe-LDHm. (c) N_2 adsorption and desorption isotherms at 77 K and (d) corresponding pore size distributions of CuFe-LDHs, CuFe-LDHm and Pt@CuFe-LDHm. (e) AFM image and (f) the corresponding height profile of Pt@CuFe-LDHm.

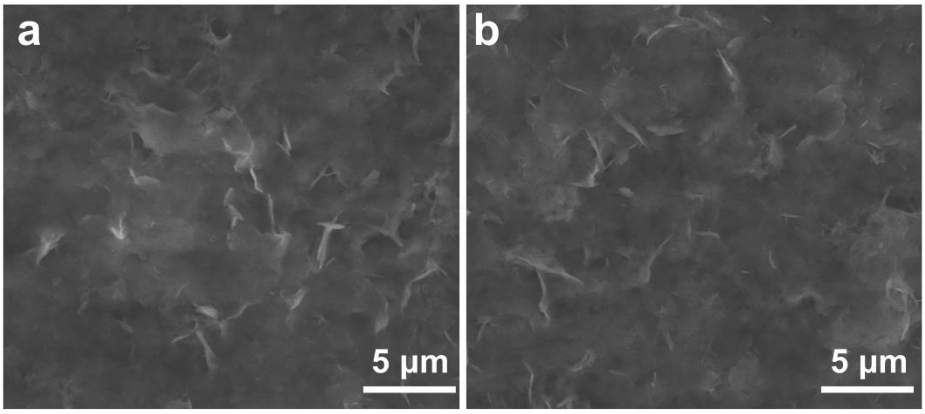

Fig. S2. The FESEM images of (a) CuFe-LDHs-sheet and (b) Pt@CuFe-LDHs-sheet.

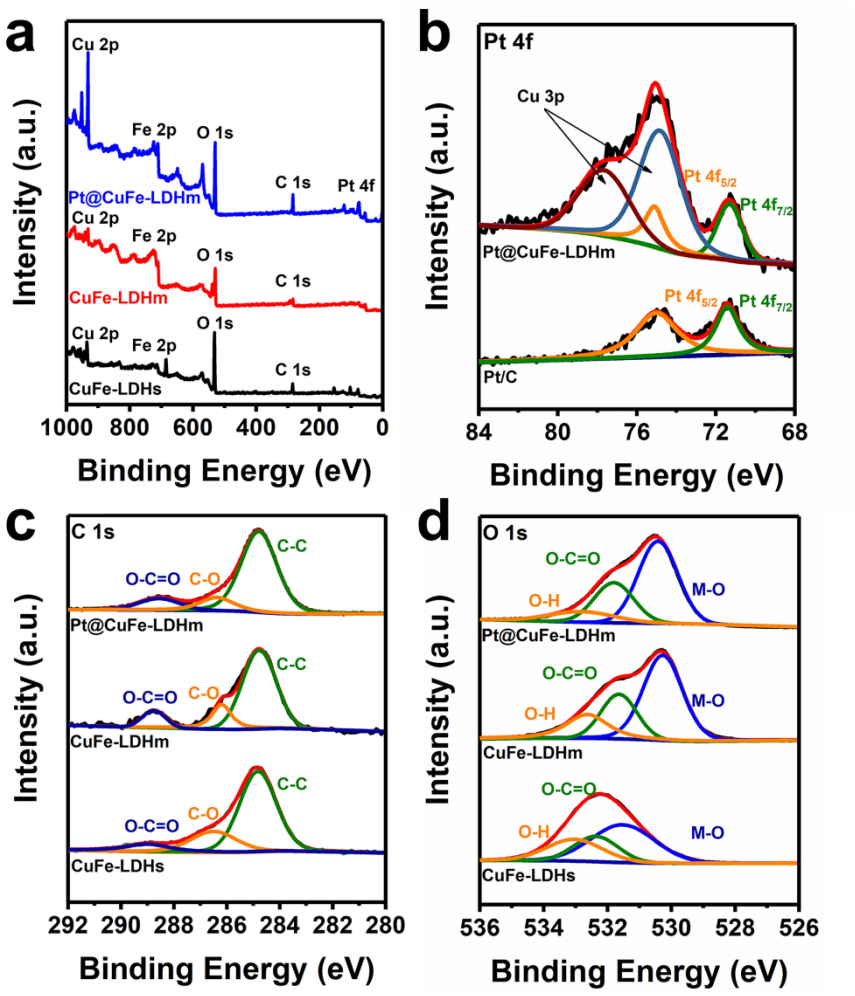

Fig. S3. (a) XPS survey spectra for CuFe-LDHs, CuFe-LDHm and Pt@CuFe-LDHm. High-resolution XPS spectra of (b) Pt 4f for Pt@CuFe-LDHm. High-resolution XPS spectra of (c) C 1s and (d) O 1s for CuFe-LDHs, CuFe-LDHm and Pt@CuFe-LDHm.

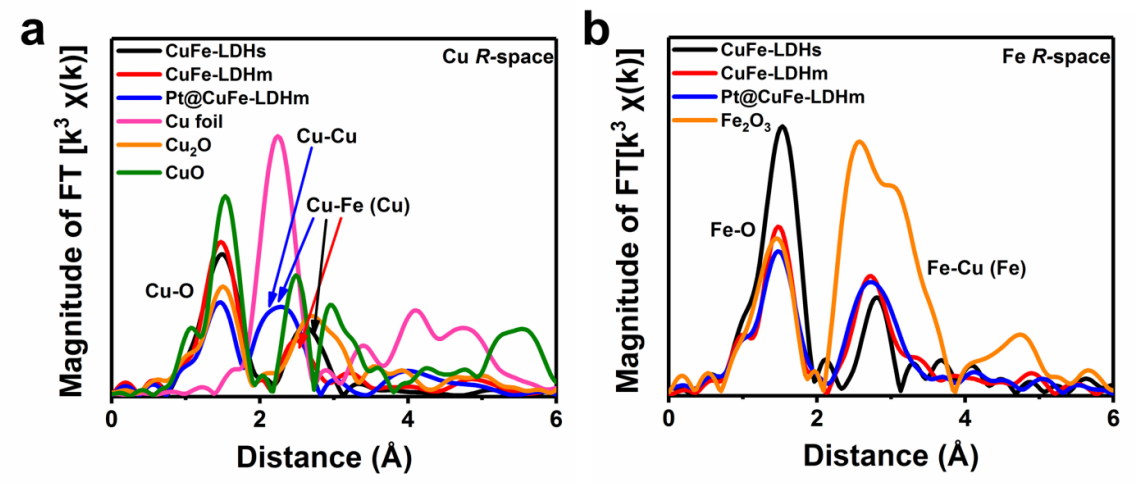

Fig. S4. Fourier transform EXAFS spectra of (a) Cu *R*-space and (b) Fe *R*-space for CuFe-LDHs, CuFe-LDHm and Pt@CuFe-LDHm.

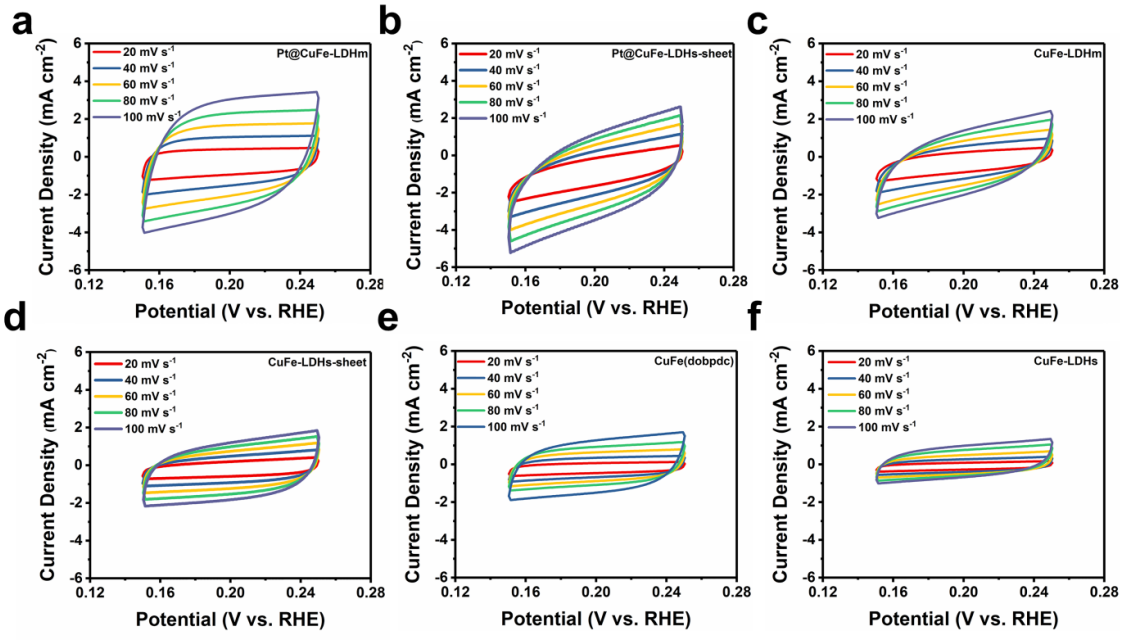

Fig. S5. CV curves between 0.15 and 0.25 V vs RHE in 1.0 M KOH electrolyte for (a) Pt@CuFe-LDHm, (b) Pt@CuFe-LDHs-sheet, (c) CuFe-LDHm, (d) CuFe-LDHs-sheet, (e) CuFe(dobpdc) and (f) CuFe-LDHs.

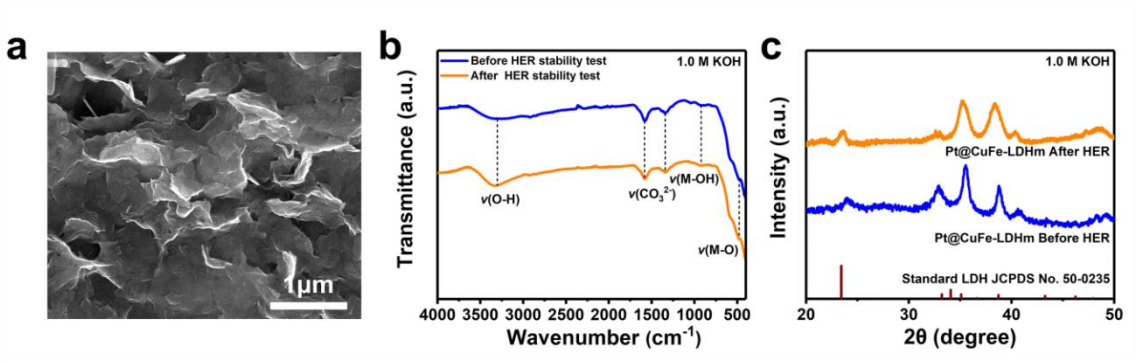

Fig. S6. (a) FESEM image, (b) FTIR spectra and (c) PXRD pattern of Pt@CuFe-LDHm after long-term electrocatalytic HER in 1.0 M KOH electrolyte.

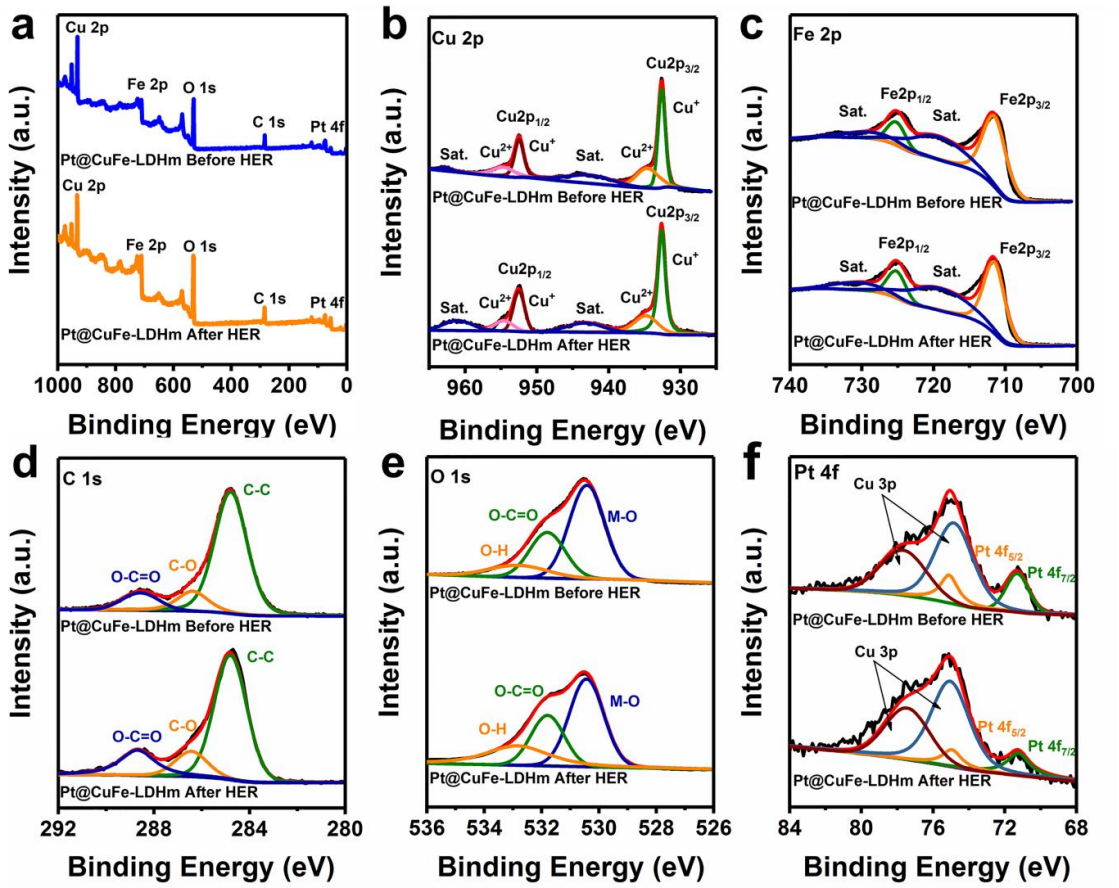

Fig. S7. (a) Survey XPS spectra and high-resolution XPS spectra of (b) Cu 2p, (c) Fe 2p, (d) C 1s, (e) O 1s and (f) Pt 4f of Pt@CuFe-LDHm before and after the long-term electrocatalytic HER in 1.0 M KOH electrolyte.

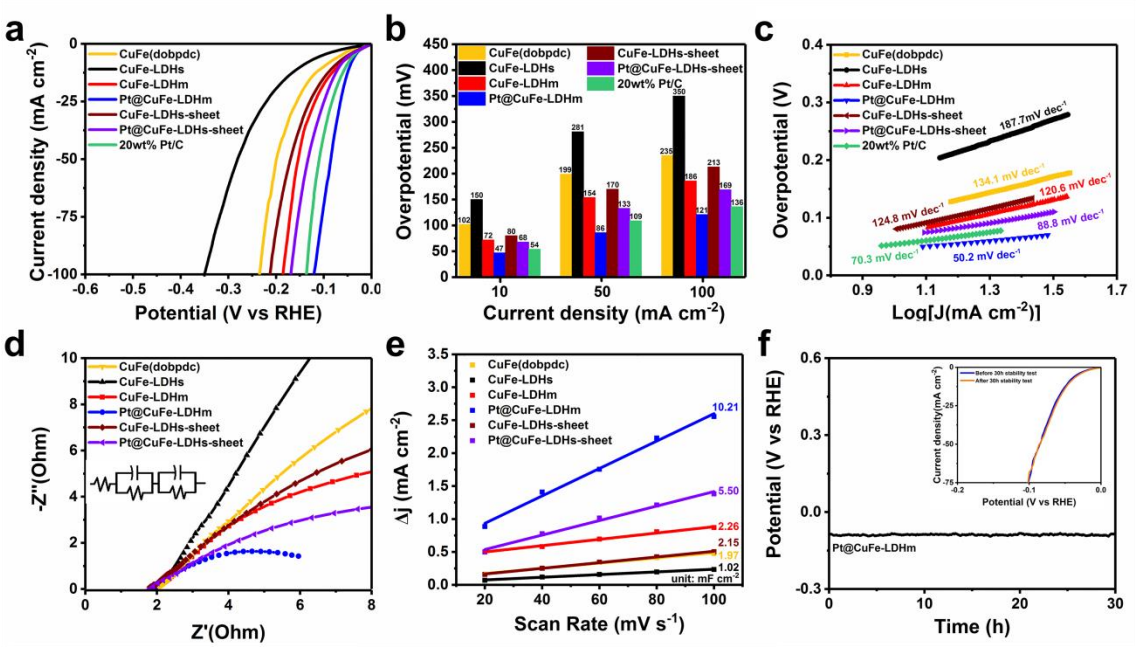

Fig. S8. The HER performance of CuFe(dobpdc), CuFe-LDHs, CuFe-LDHm, Pt@CuFe-LDHm, CuFe-LDHs-sheet and Pt@CuFe-LDHs-sheet in 0.1 M KOH electrolyte. (a) LSV curves, (b) overpotentials at current densities of 10, 50 and 100 mA cm^{-2}, (c) Tafel slopes, (d) Nyquist plots and (e) C_{dl} calculations by plotting current densities at 0.2 V vs RHE as function of scan rates. (f) Chronopotentiometry test for Pt@CuFe-LDHm at a constant current density of 10 mA cm^{-2} for 30 h. Inset shows the LSV curves before and after the long-term HER electrolysis of Pt@CuFe-LDHm in 0.1 M KOH solution.

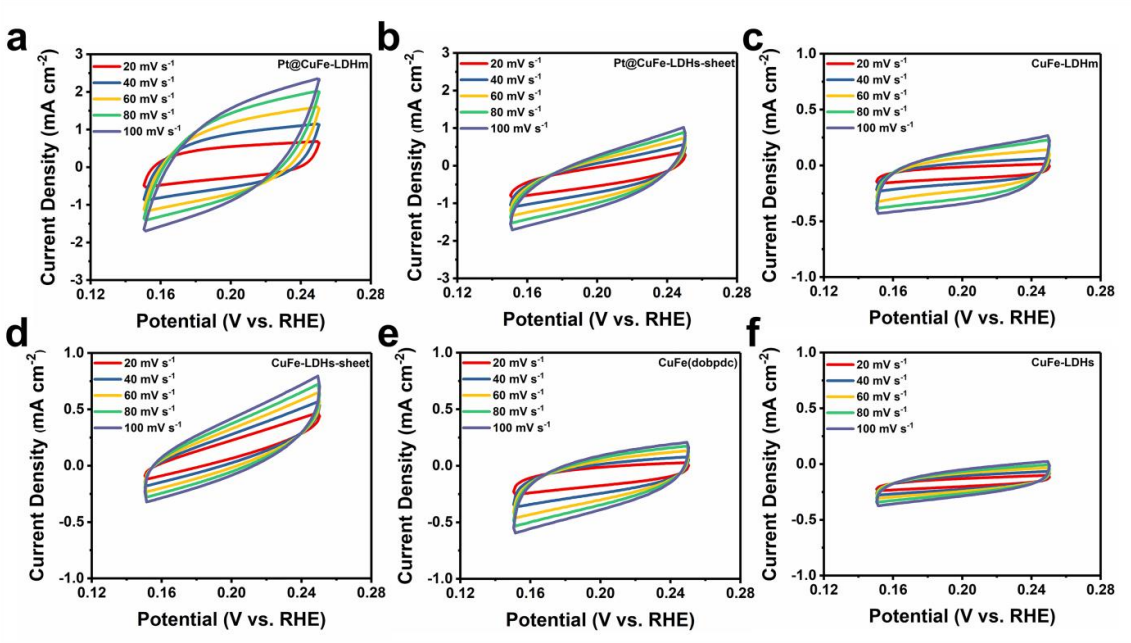

Fig. S9. CV curves between 0.15 and 0.25 V vs RHE in 0.1 M KOH electrolyte for (a) Pt@CuFe-LDHm, (b) Pt@CuFe-LDHs-sheet, (c) CuFe-LDHm, (d) CuFe-LDHs-sheet, (e) CuFe(dobpdc) and (f) CuFe-LDHs.

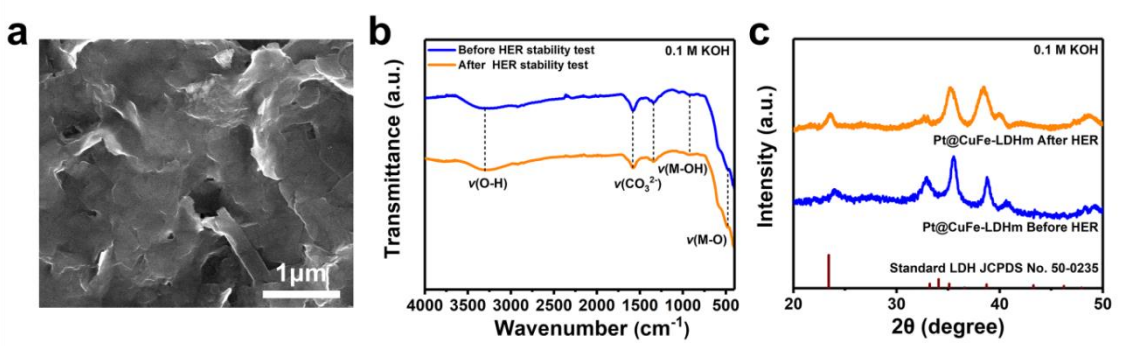

Fig. S10. (a) FESEM image, (b) FTIR spectra and (c) PXRD pattern of Pt@CuFe-LDHm after long-term electrocatalytic HER in 0.1 M KOH electrolyte.

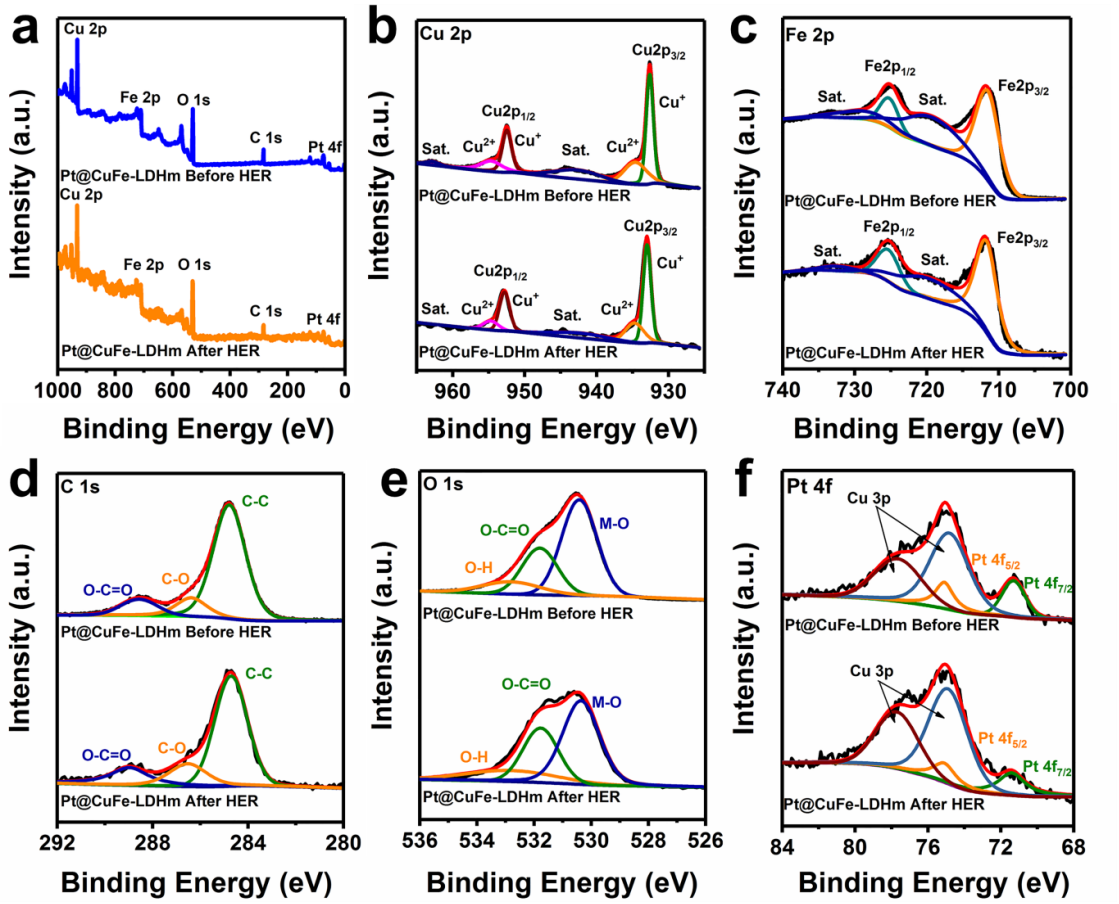

Fig. S11. (a) Survey XPS spectra and high-resolution XPS spectra of (b) Cu 2p, (c) Fe 2p, (d) C 1s, (e) O 1s and (f) Pt 4f of Pt@CuFe-LDHm before and after the long-term electrocatalytic HER in 0.1 M KOH electrolyte.

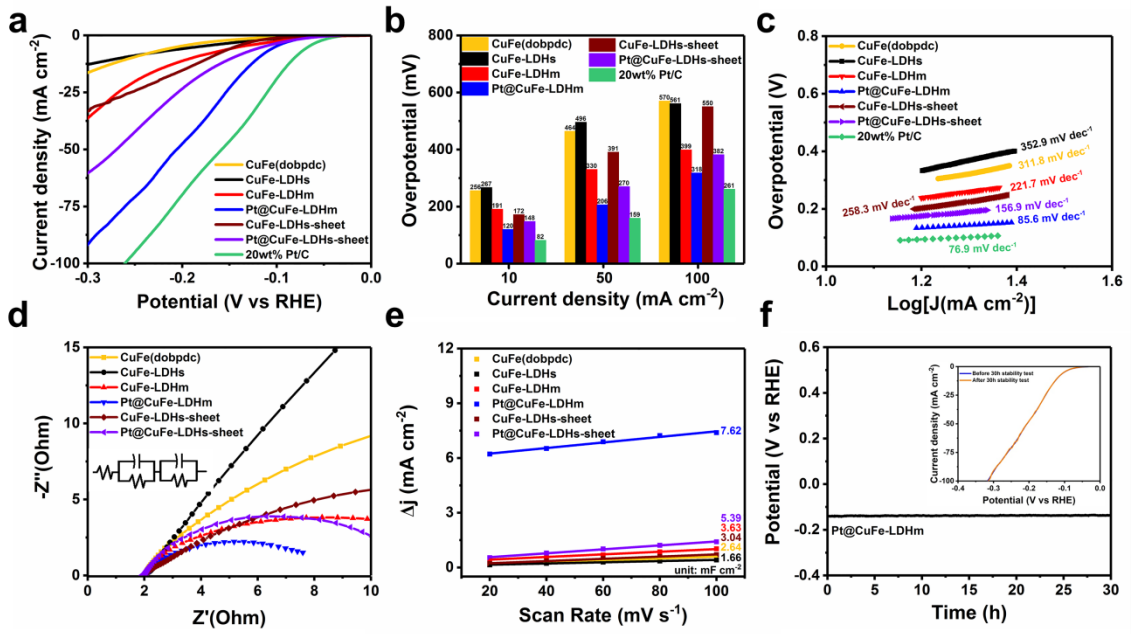

Fig. S12. The HER performance of CuFe(dobpdc), CuFe-LDHs, CuFe-LDHm, Pt@CuFe-LDHm, CuFe-LDHs-sheet and Pt@CuFe-LDHs-sheet in 1.0 M PBS electrolyte. (a) LSV curves, (b) overpotentials at current densities of 10, 50 and 100 mA cm^{-2}, (c) Tafel slopes, (d) Nyquist plots and (e) C_{dl} calculations by plotting current densities at 0.2 V vs RHE as function of scan rates. (f) Chronopotentiometry test for Pt@CuFe-LDHm at a constant current density of 10 mA cm^{-2} for 30 h. Inset shows the LSV curves before and after the long-term HER electrolysis of Pt@CuFe-LDHm in 1.0 M PBS solution.

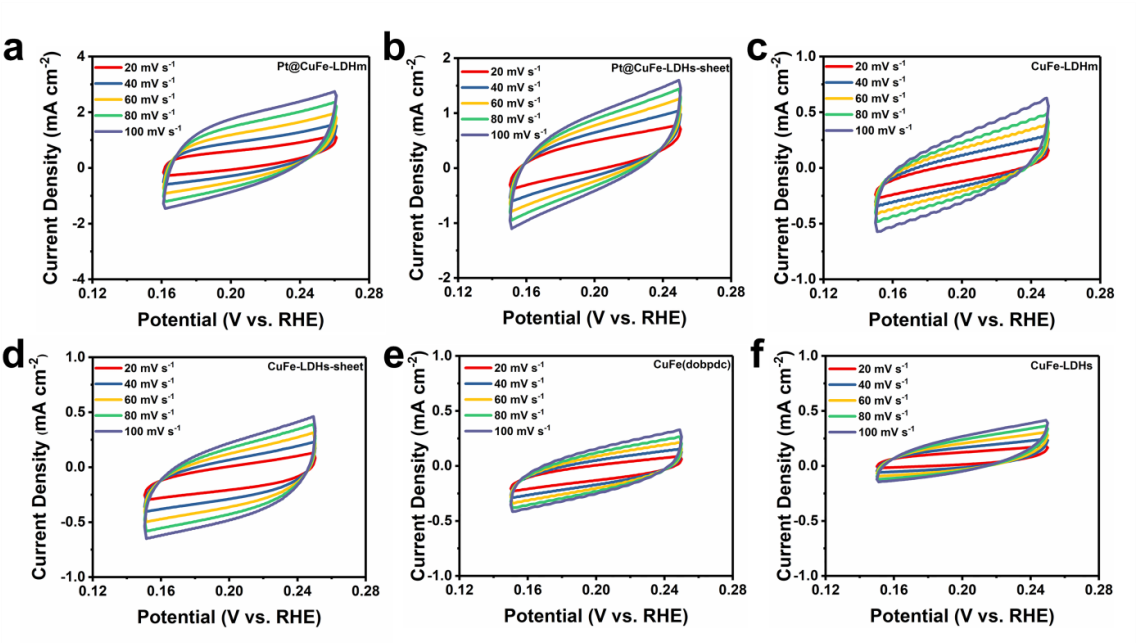

Fig. S13. CV curves between 0.15 and 0.25 V vs RHE in 1.0 M PBS electrolyte for (a) Pt@CuFe-LDHm, (b) Pt@CuFe-LDHs-sheet, (c) CuFe-LDHm, (d) CuFe-LDHs-sheet, (e) CuFe(dobpdc) and (f) CuFe-LDHs.

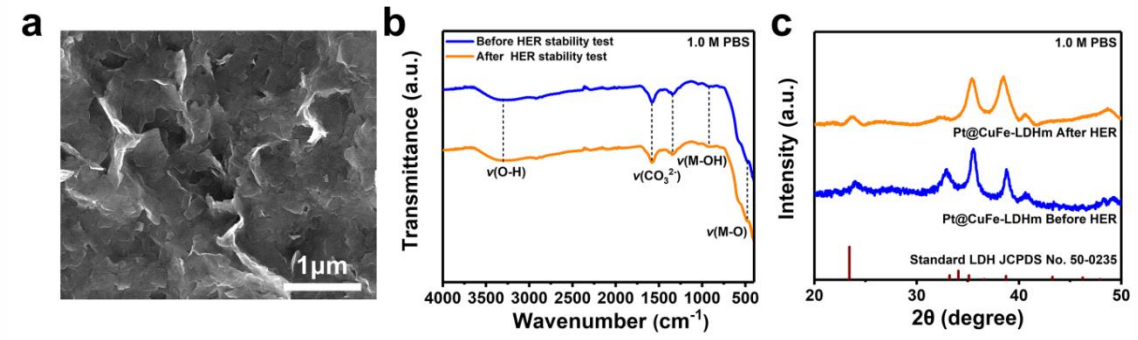

Fig. S14. (a) FESEM image, (b) FTIR spectra and (c) PXRD pattern of Pt@CuFe-LDHm after long-term electrocatalytic HER in 1.0 M PBS electrolyte.

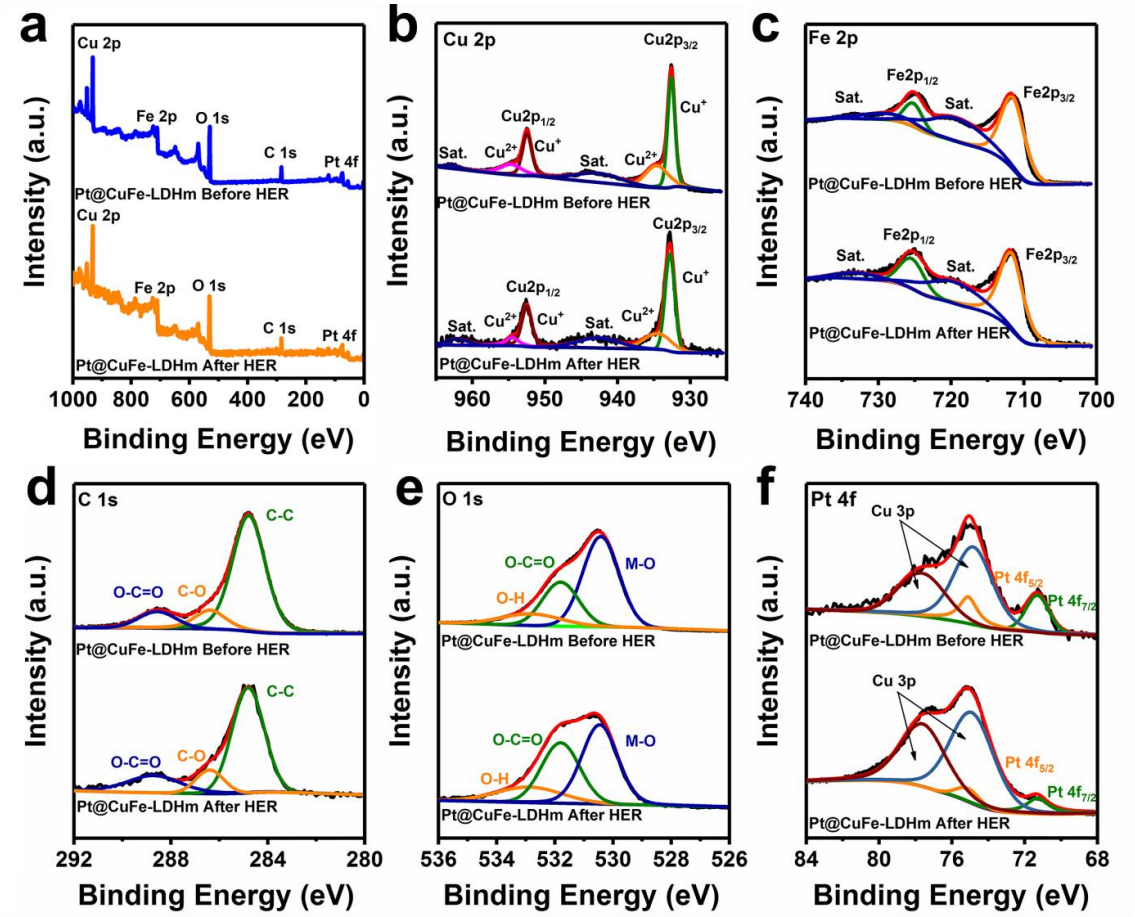

Fig. S15. (a) Survey XPS spectra and high-resolution XPS spectra of (b) Cu 2p, (c) Fe 2p, (d) C 1s, (e) O 1s and (f) Pt 4f of Pt@CuFe-LDHm before and after the long-term electrocatalytic HER in 1.0 M PBS electrolyte.

3. Supplementary Tables

Table S1 The contents of metal elements in CuFe-LDHs, CuFe-LDHm and Pt@CuFe-LDHm analyzed by ICP-OES.[2,3]

Samples	Cu (wt %)	Fe (wt %)	Pt (wt %)	Cu/Fe molar ratio
CuFe-LDHs	42.5	21.4	-	1.8 : 1
CuFe-LDHm	42.6	20.1	-	1.8 : 1
Pt@CuFe-LDHm	41.6	21.6	1.1	1.7 : 1

Table S2. BET surface area and pore size of Pt@CuFe-LDHm and other recently reported electrocatalysts.

Electrocatalysts	BET surface area ($m^2 g^{-1}$)	Pore size (nm)	References
CuFe-LDHm	**90**	**27**	
Pt@CuFe-LDHm	**84**	**27**	**This work**
CuFe-LDHs	**38**	**1.4-9**	
CoNi-LDH	10.3	25	4
MgAl-LDH	18.6	12.5	5
CoFe-LDH	76.0	2-10	6
CoFe-LDH	50.1	7.6	7

Table S3. Electrocatalytic HER performance of Pt@CuFe-LDHm and other recently reported HER electrocatalysts.

Electrocatalysts	Electrolytes	Overpotentials (mV @ mA cm^{-2})	Tafel slopes (mV dec^{-1})	References
Pt@CuFe-LDHm	**1.0 M KOH**	**33 @ 10**	**34.0**	**This work**
	0.1 M KOH	**47 @ 10**	**50.2**	
	1.0 M PBS	**120 @ 10**	**85.6**	
CuFe-LDHm	**1.0 M KOH**	**63 @ 10**	**40.9**	
	0.1 M KOH	**71 @ 10**	**120.6**	
	1.0 M PBS	**191 @ 10**	**221.7**	
CuFe-LDH/NF	1.0 M NaOH	159 @ 10	123.0	8
CuFe-P/NF	1.0 M KOH	153 @ 10	125.4	9
$Fe(OH)_x$@Cu-MOF	1.0 M KOH	112 @ 10	76.0	10
$Cu_{0.50}Fe_{0.50}$/NF	1.0 M KOH	158 @ 10	62.2	11
$Fe(PO_3)_2$@Cu_3P	1.0 M KOH	108 @ 10	84.0	12
$Cu_{2.75}Fe_{0.25}P$	1.0 M KOH	158 @ 100	67.5	13
$NiCu_{0.05}Fe_{0.025}$	1.0 M KOH	60 @ 10	60.8	14
FeCoCuP@NC	1.0 M KOH	169 @ 10	48.8	15
Fe-Cu@CN_3	1.0 M KOH	91 @ 10	117.0	16
$Fe_{0.43}Co_{2.57}(PO_4)_2$/Cu	1.0 M KOH	108 @ 100	30.3	17
ZIF@LDH@Ni foam-600	1.0 M KOH	106 @ 10	109.0	18
NiFe-LDH + 2D-Pt	1.0 M KOH	61 @ 100	32.3	19
$V_{0.3}$-CoFe-LDH	1.0 M KOH	98 @ 10	78.0	20
Rh-doped CoFe-LDH	1.0 M KOH	75 @ 10	42.8	21
Ni-Fe-Pt NCs	1.0 M KOH	463 @ 10	81.0	22
PtCu-MoO_2@C	1.0 M KOH	37 @ 10	36.0	23
Ni-MOF@Pt	1.0 M KOH	102 @ 10	88.0	24
NiVB/rGO	0.1 M KOH	315 @ 10	128.0	25
NiFe LDH-POM	0.1 M KOH	156 @ 10	86.0	26
Ni-Fe clusters	0.1 M KOH	71 @ 10	-	27
C-ZIF-CuPt	0.1 M KOH	46 @ 10	45.0	28
Cu-Ni_3S_2	1.0 M PBS	228 @ 10	151.0	29
Cu-CoP NRAs/CC	1.0 M PBS	137 @ 10	144.0	30
$Cu(OH)_2$NRs@$Ni(OH)_2$NSs	1.0 M PBS	200 @ 10	120.0	31
GO-Fe,Ni HHNs	1.0 M PBS	190 @ 10	110.0	32
Fe-Mo_2C@NCF	1.0 M PBS	130 @ 10	109.0	33
Co-Fe-P nanotubes	1.0 M PBS	138 @ 10	138.0	34
Fe-Co-Ni-B/BVG	1.0 M PBS	168 @ 10	42.0	35
Mn-FeP	1.0 M PBS	157 @ 10	78.0	36
FeP NPs@NPC	1.0 M PBS	386 @ 10	149.0	37
S-$NiFe_2O_4$	1.0 M PBS	197 @ 10	81.3	38

Table S4. Comparison of the onset potentials of prepared electrocatalysts in 1.0 M KOH, 0.1 M KOH and 1.0 M PBS.

Onset Potential (mV)	1.0 M KOH	0.1 M KOH	1.0 M PBS
Pt@CuFe-LDHm	1.6	8.8	61.8
CuFe-LDHm	3.6	10.8	68.0
Pt@CuFe-DHs-sheet	1.7	9.5	64.0
CuFe-DHs-sheet	4.6	11.4	98.0
CuFe-LDHs	50.6	26.8	88.0
CuFe(dobpdc)	57.6	12.8	117.0

References

1 C. W. Pao, J. L. Chen, J. F. Lee, M. C. Tsai, C. Y. Huang, C. C. Chiu and Y. S. Huang, *J. Synchrotron Rad.*, 2021, **28**, 930-938.
2 H. Yang, T. Guo, D. Yin, Q. Liu, X. Zhang and X. Zhang, *J. Taiwan Inst. Chem. E.*, 2020, **112**, 212-221.
3 F. Dionigi, J. Zhu, Z. Zeng, T. Merzdorf, H. Sarodnik, M. Gliech, L. Pan, W. Li, J. Greeley and P. Strasser, *Angew. Chem. Int. Ed.*, 2021, **133**, 14567-14578.
4 L. Xie, S. Chen, Y. Hu, Y. Lan, X. Li, Q. Deng, J. Wang, Z. Zeng and S. Deng, *J. Alloy. Compd.*, 2021, **858**, 157652.
5 L. D. Silva Neto, C. G. Anchieta, J. L. S. Duarte, L. Meili and J. T. Freire, *ACS Omega*, 2021, **6**, 21819-21829.
6 L. Han, C. Dong, C. Zhang, Y. Gao, J. Zhang, H. Gao, Y. Wang and Z. Zhang, *Nanoscale*, 2017, **9**, 16467-16475.
7 B. Wang, W. X. Lu, Z. Q. Huang, D. S. Pan, L. L. Zhou, Z. H. Guo and J. L. Song, *Chem. Eng. J.*, 2020, **399**, 125799.
8 M. Bhavanari, K. R. Lee, C. J. Tseng, I. H. Tang and H. H. Chen, *Int. J. Hydrog. Energy*, 2021, **46**, 35886-35895.
9 X. Xing, Y. Song, W. Jiang and X. Zhang, *Sustain. Energ. Fuels*, 2020, **4**, 3985-3991.
10 W. Cheng, H. Zhang, D. Luan and X. W. Lou, *Sci. Adv.* 2021, **7**, 2580.
11 A. I. Inamdar, H. S. Chavan, B. Hou, C. H. Lee, S. U. Lee, S. Cha, H. Kim and H. Im, *Small*, 2020, **16**, 1905884.
12 D. Dai, B. Wei, Y. Li, X. Ma, S. Liang, S. Wang and L. Xu, *J. Alloy. Compd.*, 2020, **820**, 153185.
13 I. Mondal, A. Mahata, H. Kim, U. Pal, F. De Angelis and J. Y. Park, *Nanoscale,* 2020, **12**, 17769-17779.
14 C. Hegde, X. Sun, K. N. Dinh, A. Huang, H. Ren, B. Li, R. Dangol, C. Liu, Z. Wang, Q. Yan and H. Li, *ACS Appl. Mater. Interfaces*, 2020, **12**, 2380-2389.
15 S. Li, Q. Zhang, J. Sun and J. Guan, *Mater. Today Energy*, 2020, **17**, 100464.
16 Q. He, H. Liu, P. Tan, J. Xie, S. Si and J. Pan, *J. Solid State Chem*, 2021, **299**, 122179.
17 C. Yang, T. He, W. Zhou, R. Deng and Q. Zhang, *ACS Sustain. Chem. Eng.*, 2020, **8**, 13793-13804.
18 Y. Tang, X. Fang, X. Zhang, G. Fernandes, Y. Yan, D. Yan, X. Xiang and J. He, *ACS Appl. Mater. Interfaces*, 2017, **9**, 36762-36771.

19 S. W. Jang, S. Dutta, A. Kumar, Y. R. Hong, H. Kang, S. Lee, S. Ryu, W. Choi and I. S. Lee, *ACS Nano*, 2020, **14**, 10578-10588.
20 B. Singh and A. Indra, *Dalton Trans*, 2021, **50**, 2359-2363.
21 K. Zhu, J. Chen, W. Wang, J. Liao, J. Dong, M. O. L. Chee, N. Wang, P. Dong, P. M. Ajayan, S. Gao, J. Shen and M. Ye, *Adv. Funct. Mater.*, 2020, **30**, 2003556.
22 M. Fu, Q. Zhang, Y. Sun, G. Ning, X. Fan, H. Wang, H. Lu, Y. Zhang and H. Wang, *Int. J. Hydro. Energy*, 2020, **45**, 20832-20842.
23 C. Zhang, P. Wang, W. Li, Z. Zhang, J. Zhu, Z. Pu, Y. Zhao and S. Mu, *J. Mater. Chem. A*, 2020, **8**, 19348-19356.
24 K. Rui, G. Zhao, M. Lao, P. Cui, X. Zheng, X. Zheng, J. Zhu, W. Huang, S. X. Dou and W. Sun, *Nano Lett.*, 2019, **19**, 8447-8453.
25 M. Arif, G. Yasin, M. Shakeel, M. A. Mushtaq, W. Ye, X. Fang, S. Ji and D. Yan, *J. Energy Chem.*, 2021, **58**, 237-246.
26 C. Li, Z. Zhang and R. Liu, *Small*, 2020, **16**, 2003777.
27 S. Xue, R. W. Haid, R. M. Kluge, X. Ding, B. Garlyyev, J. Fichtner, S. Watzele, S. Hou and A. S. Bandarenka, *Angew. Chem. Int. Ed.*, 2020, **59**, 10934-10938.
28 C. Wang, L. Kuai, W. Cao, H. Singh, A. Zakharov, Y. Niu, H. Sun and B. Geng, *Chem. Eng. J.*, 2021, **426**, 130749.
29 L. Zhang, X. Gao, Y. Zhu, A. Liu, H. Dong, D. Wu, Z. Han, W. Wang, Y. Fang, J. Zhang, Z. Kou, B. Qian and T. T. Wang, *Nanoscale*, 2021, **13**, 2456-2464.
30 L. Wen, Y. Sun, C. Zhang, J. Yu, X. Li, X. Lyu, W. Cai and Y. Li, *ACS Appl. Energy Mater.*, 2018, **1**, 3835-3842.
31 J. Hu and Y. Liu, *ChemistrySelect*, 2021, **6**, 4129-4134.
32 J. Hu and Y. Liu, *Mater. Res. Express*, 2021, **8**, 035506.
33 J. Huang, J. Wang, R. Xie, Z. Tian, G. Chai, Y. Zhang, F. Lai, G. He, C. Liu, T. Liu, P. R. Shearing and D. J. L. Brett, *J. Mater. Chem. A*, 2020, **8**, 19879-19886.
34 J. Chen, J. Liu, J. Q. Xie, H. Ye, X. Z. Fu, R. Sun and C. P. Wong, *Nano Energy*, 2019, **56**, 225-233.
35 Y. Man, F. Shaik, B. Jiang and J. Zheng, *J. Electrochem. Soc.*, 2020, **167**, 122513.
36 M. Wang, Y. Tuo, X. Li, Q. Hua, F. Du and L. Jiang, *ACS Sustain. Chem. Eng.*, 2019, **7**, 12419.
37 Z. Pu, I. S. Amiinu, C. Zhang, M. Wang, Z. Kou and S. Mu, *Nanoscale*, 2017, **9**, 3555-3560.
38 J. Liu, D. Zhu, T. Ling, A. Vasileff and S. Z. Qiao, *Nano Energy*, 2017, **40**, 264-273.